INSTITUTE OF PHYSICS PUBLISHING and INTERNATIONAL ATOMIC ENERGY AGENCY NUCLEAR FUSION

Nucl. Fusion **45** (2005) 1321–1327 doi:10.1088/0029-5515/45/11/013

Transport phenomena in the edge of Alcator C-Mod plasmas

J.L. Terry[1], N.P. Basse[1], I. Cziegler[1], M. Greenwald[1], O. Grulke[2], B. LaBombard[1], S.J. Zweben[3], E.M. Edlund[1], J.W. Hughes[1], L. Lin[1], Y. Lin[1], M. Porkolab[1], M. Sampsell[4], B. Veto[1] and S.J. Wukitch[1]

[1] Plasma Science and Fusion Center, MIT, Cambridge, MA 02139-4307, USA
[2] MPI for Plasma Physics, EURATOM Association and Ernst-Moritz-Arndt University, Greifswald, Germany
[3] Princeton Plasma Physics Laboratory, Princeton, NJ 08543, USA
[4] Fusion Research Center, The University of Texas at Austin, Austin, TX 78712, USA

E-mail: terry@psfc.mit.edu

Received 13 December 2004, accepted for publication 5 August 2005
Published 24 October 2005
Online at stacks.iop.org/NF/45/1321

Abstract
Two aspects of edge turbulence and transport in Alcator C-Mod are explored. The quasi-coherent mode (QCM), an edge fluctuation present in Enhanced Dα H-mode plasmas, is examined with regard to its role in the enhanced particle transport found in these plasmas, its in/out asymmetry, its poloidal wave number and its radial width and location. It is shown to play a dominant role in the perpendicular particle transport. The QCM is not observed at the inboard midplane, indicating that its amplitude there is significantly smaller than on the outboard side. The peak amplitude of the QCM is found just inside the separatrix, with a radial width $\gtrsim$5 mm, leading to a non-zero amplitude outside the separatrix and qualitatively consistent with its transport enhancement. Also examined are the characteristics of the intermittent convective transport, associated with the larger scale turbulent structures, also called blobs, and typically occurring in the scrape-off-layer (SOL). These turbulent structures are qualitatively similar in L- and H-mode. When their perpendicular extent, occurrence frequencies and magnitudes are compared, it is found that their size is somewhat smaller in ELMfree H-Mode, while their frequency is similar. A clear difference is seen in the magnitude of these turbulent fluctuations in the far SOL, with ELMfree H-mode showing a smaller perturbation there than L-mode. As the Greenwald density limit is approached ($n/n_{\mathrm{GW}} \geqslant 0.7$), blobs are seen inside the separatrix consistent with the observation that the high cross-field transport region, normally found in the far SOL, penetrates the closed flux surfaces at high n/n_{GW}.

PACS numbers: 52.35.R, 52.70, 52.55, 52.40.H

(Some figures in this article are in colour only in the electronic version)

1. Introduction

Transport in the edge and scrape-off-layer (SOL) can play a crucial role in overall plasma confinement, for example, through the formation and character of the H-mode edge transport barrier or as a key aspect of the density limit [1]. The research described here concentrates on two phenomena observed in the edge and SOL of Alcator C-Mod plasmas, both involved with cross-field particle transport. The first phenomenon is the quasi-coherent mode (QCM) fluctuation that is observed in Enhanced Dα (EDA) H-mode plasmas [2], while the second is the intermittent convective turbulence [3], often identified as blobs, typically associated with the far SOL and enhanced main chamber recycling. In the case of the QCM, after showing evidence that it is largely responsible for the enhanced particle transport in EDA H-mode, we will address the inboard–outboard asymmetry of its magnitude, its radial width and location at the outboard midplane and its poloidal wave number. The importance of the intermittent blob transport derives from the fact that the cross-field particle fluxes it drives can be greater than the parallel fluxes [4], with significant implications for recycling and divertor design. It has also been implicated as playing an important role in the density limit [1]. We will discuss the in/out asymmetry of the broadband fluctuations dominated by the blobs, as well as characterize the similarities and differences of the blob

turbulence in C-Mod's L- and H-mode plasmas. Finally, we will present observations of blobs being generated *inside* the separatrix as the density limit is approached, thereby supporting the hypothesis that the penetration of blob transport into the closed flux surfaces may be related to the density limit.

2. Experimental diagnostics

The primary diagnostics used to characterize the two edge phenomena of interest here are the optical 'gas-puff-imaging' (GPI) diagnostics, the phase-contrast-imaging (PCI) diagnostic, and scanning Langmuir probes. While the QCM is readily observable by a number of other diagnostics, e.g. reflectometry, BES and magnetic pick-up coils mounted in a scanning probe head, we discuss characteristics of the mode as measured by the GPI optical diagnostics and PCI. In determining characteristics of the blob turbulence, we use measurements from the GPI and the scanning Langmuir probes.

GPI [5–7] was developed in order to study edge turbulence. With this technique, emission is localized in the toroidal dimension, thereby overcoming a disadvantage of line-of-sight-integrating, passive optical diagnostics. With GPI, emission (D_α or He I) from a localized gas-puff is made to be much greater (typically $\geqslant 5\times$) than any intrinsic emission along the line-of-sight. Since the gas-puff emission is viewed along the sight lines that are configured to cross it, spatial localization is provided. In C-Mod gas-puff barrels are located on both inboard and outboard sides, near the plasma midplane and typically only 1–3 cm from the separatrix. The outboard gas-puff is viewed by two arrays—one made up of discrete fibres whose focal spots are arranged in a radial array in front of the barrel. The focal spots are typically 4–5 mm in diameter and together span the plasma edge. The fibres transmit light to photodiodes filtered for D_α and with a flat frequency response for frequencies $\leqslant$250 kHz. A coherent fibre bundle is also employed to image the emission in two-dimensional in front of the outboard barrel. Since its view is parallel to the magnetic field at the gas-puff location, it images the structure of the emission perpendicular to the field. The two-dimensional image is transmitted to a 300 frame movie camera with a maximum frame rate of 250 kHz. The camera's 64 × 64 pixel array, in combination with the imaging optics, yields ∼3 mm spatial resolution in the plasma [8]. Both these GPI systems detect the QCM and the blobs. The inboard gas-puff is viewed by another radially-resolving array of fibres. These array-views span the inboard separatrix and are used for comparing with observations from the outboard side. It is important to remember that the GPI technique measures the effects of the underlying density and temperature turbulence on *emission*, since it is sensitive to both [9]. Nonetheless, neither density nor temperature fluctuations are being measured directly.

3. Characteristics of the QCM

EDA H-mode confinement in C-Mod is distinguished by good energy confinement, but with enough particle transport that the density does not increase monotonically and impurities do not accumulate, as occurs in ELMfree H-mode. The enhanced particle transport appears to be provided by the QCM, a fluctuation that is localized to the edge region. The QCM is a fluctuation of density, potential and magnetic field [10], with a frequency spectrum peaked typically between 90 and 200 kHz. The evidence that the QCM is responsible for the enhanced transport is (1) the magnitude of the oscillation is observed to increase the time-averaged 'effective particle diffusion coefficient', $D_{\rm eff}$ (defined below), and (2) the absence of the fluctuation in ELMfree H-modes, in which both density and impurities accumulate. The first statement is illustrated in figure 1, where $D_{\rm eff} \equiv -\Gamma_{\rm perp}/\nabla n_{\rm e}$, is plotted versus the QCM amplitude. $D_{\rm eff}$ is determined from probe measurements of $\nabla n_{\rm e}$, with $\Gamma_{\rm perp}$ inferred [11] from spatially-resolved measurements of the ionization source, including the effects of parallel plasma flows towards the divertor. (Note that the use of $D_{\rm eff}$ is not meant to imply that the transport is wholly or even primarily diffusive.) The QCM amplitude is measured by the PCI diagnostic which measures line integrated density fluctuations along 12 vertical chords that together span a ∼4 cm section of radial width, crossing the midplane near the plasma centre [10]. Only the observed *trend* of increasing $D_{\rm eff}$ with QCM density fluctuation amplitude is significant, primarily because of the relatively few data points and the uncertainties in the $D_{\rm eff}$ determination.

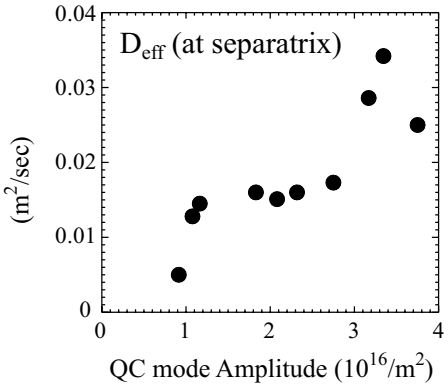

Figure 1. Increase of $D_{\rm eff}$ with the increase of the QCM amplitude. Here $D_{\rm eff} \equiv -\Gamma_{\rm perp}/\nabla n_{\rm e}$, where $\nabla n_{\rm e}$ is determined from probe measurements and $\Gamma_{\rm perp}$ is inferred from spatially-resolved measurements of the ionization source. The QCM amplitude is the line integral of the density fluctuation within the QCM frequency feature.

Because of the primary role of the QCM in the particle transport out of the pedestal, and because the QCM is still not understood theoretically, we have investigated a number of its characteristics. The first is its poloidal character. It is known that the QCM is localized to the edge region, at least on the outboard side, as documented by probes [12, 13], BES [14] and reflectometry [2]. In addition, the PCI measurements of the mode are consistent with its existence at the *top* and *bottom* edge of the plasma at major radii near the plasma centre but still outboard of the x-point. The outboard GPI arrays also detect the QCM since its density fluctuation is manifested as an emission fluctuation. An example of the frequency spectrum of GPI emission from 50 to 250 kHz is shown in figure 2(*a*). The emission is detected by one of the radial array views, viewing the puff at $\rho \sim -7$ mm, i.e. ∼7 mm inside the separatrix. (ρ is the radial distance beyond the separatrix of a given point when flux-surface-mapped to

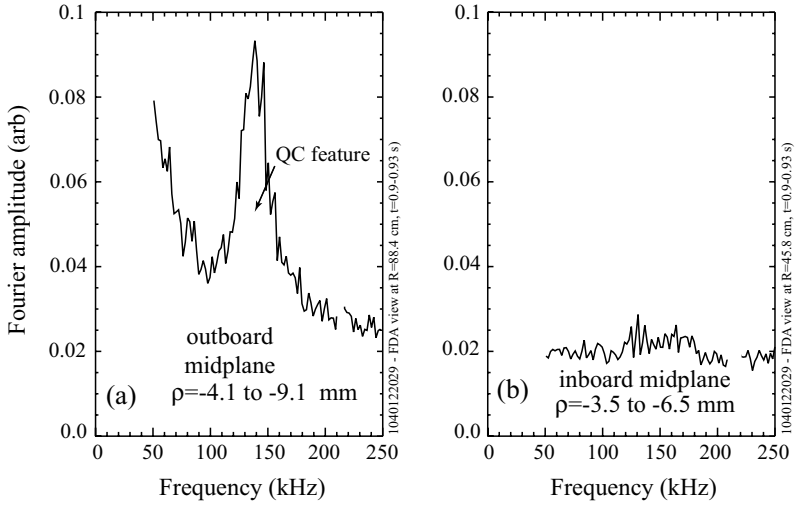

Figure 2. (*a*) QCM feature as observed on a single outboard view; such a feature is seen on views spanning $-13 < \rho < 3$ mm (spot sizes $\sim$5 mm). (*b*) Same spectral region (at the same time) for fluctuations from a single inboard midplane view. No feature is seen for $-6.5 < \rho < 5$ mm.

the outside midplane.) In contrast, there is no evidence of the QCM feature at the *inboard* midplane, even at inboard locations that are on flux surfaces which exhibit the fluctuation on the outboard side. The absence of an inboard QCM feature is evident in figure 2(*b*), where a spectrum from one of the inboard views is shown. Thus we conclude that the QCM mode amplitude is much reduced at the inboard midplane, implying that curvature is involved in the drive for this mode.

Using the two-dimensional view of the GPI camera, we can examine the radial structure and poloidal wave number of the mode at the outboard midplane. With the camera's 250 kHz frame rate, frequencies up to 125 kHz are measurable without aliasing. The camera's view is such that it is sensitive to fluctuations with poloidal wave number in the range $0.4\,\mathrm{cm}^{-1} < |k_\theta| < 10\,\mathrm{cm}^{-1}$ (limited by the $\sim$8 cm maximum vertical extent of the view and the $\sim$0.3 cm camera resolution). The QCM is much more difficult to detect with the camera than it is by using the outboard diode array (which samples at 1 MHz for $\sim$125 ms). In fact, the frequency spectra from *individual* camera pixels (with relatively noisy 300-point time-series signals) show no clear QCM feature above the noise. In order to overcome this limitation we utilized the two-dimensional, many-pixel features of the camera images and the fact that the mode is field-aligned [10]. By averaging the (complex) frequency Fourier coefficients from those pixels viewing the same flux surface and by performing that average at different k_θ values, the QCM amplitude on the specific flux surface emerges from the noise. Spectra as functions of k_θ and f that have been determined in this way are shown in figure 3(*a*). In this case, the fluctuation is seen to have a peak amplitude at a frequency of $\sim$100 kHz and a k_θ of $\sim 1.0\,\mathrm{cm}^{-1}$. $k_\theta > 0$ indicates a wave propagating in the electron diamagnetic direction (up in the camera's view). The frequency of the feature is the same as that measured simultaneously by the PCI (figure 3(*b*)) and the outboard diode array. Figure 3(*b*) shows the (k_R, f) spectrum[1] of density

[1] Note that the PCI measures k_R, and $|k_\mathrm{R}| = |k_\theta|/\sin\zeta$, where ζ is the angle between the separatrix and the vertical at the locations where the PCI chords cross the plasma edge.

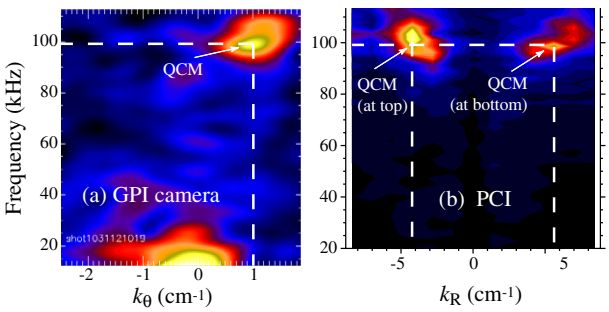

Figure 3. (*a*) QCM feature in GPI camera's (k_θ, f) spectrum measured along that fraction of the flux surface in the field-of-view having $\rho \sim -10$ mm. (*b*) QCM feature in (k_R, f) space as detected by the PCI at the same time. The colour scales are linear in Fourier amplitude.

fluctuations as measured by the PCI. The two features at $k_\mathrm{R} \sim -4$ and $\sim 5.5\,\mathrm{cm}^{-1}$ are evidence of the QCM fluctuation present in the PCI laser beam at the top edge (thus generating a $k_\mathrm{R} < 0$) and bottom edge (with $k_\mathrm{R} > 0$) of the plasma. This measurement also shows it propagating in the electron diamagnetic direction. (For a schematic of the PCI chords and QCM relative to the plasma see figure 2 in [10].) The three measurements of wave number are approximately consistent with a field-aligned mode, $\boldsymbol{k} \cdot \boldsymbol{B} = 0$, in which case k_θ varies on a flux surface as $k_\theta(\theta_1) = k_\theta(\theta_2)[(B_\theta\theta_2)/(B_\theta\theta_1)](R_2/R_1)^2$. Values of -3.7 and $4.3\,\mathrm{cm}^{-1}$ are *predicted* for k_R at the top and bottom PCI locations for a midplane $k_\theta = 1\,\mathrm{cm}^{-1}$, the value measured by the GPI. Measurements of k_θ by a probe (located $\sim$10 cm above the midplane) [12, 13] and measurements of the poloidal variation of k_θ using BES and PCI [14] have been done previously. They also show that k_θ typically varies between 0.8 and $2\,\mathrm{cm}^{-1}$ near the outboard midplane and that the poloidal variation is approximately consistent with a field-aligned mode.

Using the better spatial resolution of the camera ($\sim$3 mm, compared with $\sim$5 mm of the outboard diode array), we can characterize the radial structure of the D_α emission response

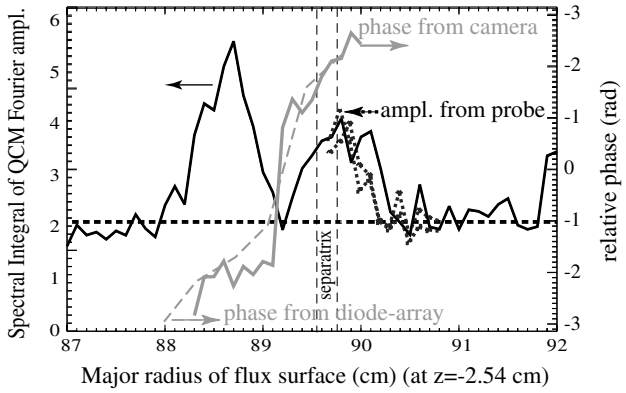

Figure 4. Radial profile of the amplitude of the GPI D_α emission at the frequency and k_{pol} of the QCM (solid dark line). This is compared with the amplitude of the QCM feature in I_{sat} as measured by the probe during a scan at the same time (thick short dashes). The two probe traces have been shifted out by 1 mm and are from the inward and outward plunges. Also shown is the relative phase as determined by the GPI camera (solid grey) and by the radial diode array (grey long dashes), shifted out by 3 mm.

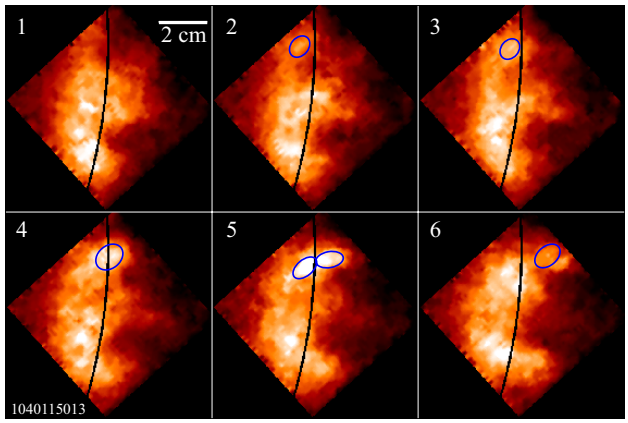

Figure 5. Movie frames of edge turbulence at $n/n_{GW} = 0.8$. The ovals locate the 'birth' and motion of a blob. The separatrix is also shown. The emission is He I, and the time between frames is 4 μs.

to QCM. By generating (k_θ, f) spectra (as in figure 3(*a*)) for different flux surfaces within the view, we calculate the maximum Fourier amplitude of the QCM feature around $f \sim 100$ kHz and $k_\theta \sim 1$ cm^{-1} versus a radial coordinate that identifies the radial location of the flux surface. Such a profile is shown in figure 4. In a similar way the radial profile of the relative phase is determined. Since the phase measurement from the camera is relatively uncertain (due to noisier data), we plot it together with that determined using diode array, whose signal-to-noise is greater but whose resolution is poorer. As shown, agreement is good. The observed radial width is significantly larger than the resolution of the camera. There appear to be two features: a larger peak of ~0.5 cm width (FWHM) which is radially inside a smaller peak of similar width. We note that the outboard diode array yields a radial profile for the mode amplitude which is consistent with that from the camera (figure 4), albeit with poorer resolution. Also shown in figure 4 is the location of the separatrix, illustrated as a stripe as a result of uncertainties due to the EFIT reconstruction (~2 mm), as well as uncertainties in the registration of the field-of-view (~2 mm). We have compared these measurements with those of the amplitude of the QCM feature in the ion saturation current as measured by the probe during a radial scan made at the same time. This is also plotted in figure 4 as the thick dashed curve. Over that portion of the profile common to both measurements, the agreement is good. Nonetheless, the fact that no probe scan has ever shown a double-peaked feature like that measured by GPI and the fact that the GPI-measured profile implies existence of the mode *inboard* of the top of the H-mode pedestal (whose density width is typically only 2–6 mm [15]) motivated us to model the response of the D_α emission to a QCM-like perturbation. This was done using the one-dimensional steady-state fluid neutrals code, KN1D [16], for which density and temperature profiles are specified and neutral profiles (and emission) are calculated. Assuming that the processes in the 'steady-state' simulation respond fast enough to model the 100 kHz QCM density oscillation, we find that an additional oscillation in the emission occurs just inboard of the emission oscillation at the radius of the modelled QCM-like density perturbation. The two oscillations in the simulation are predicted to be π radians out of phase. This is similar to what is measured (figure 4). We interpret this to be the result of ionization 'shadowing' by the density perturbation. Because the QCM feature is located well inboard of the peak in the D_α emission profile (both in the experiment and in the simulation), changes in the density profile outside of a region where the D_α emission is relatively weak can affect the emission inboard of the change. Thus we hypothesize that the second, inboard peak in the amplitude of the emission at the QCM frequency and k_{pol} may be due to this effect, while the outboard one reflects the actual QCM perturbation. Finally we point out that simulations with the BOUT turbulence code [10] yield a single radial peak with a width of ~5 mm.

These measurements make it very likely that the QCM spans the separatrix. Thus we see that the extension of the QCM onto open field lines is qualitatively consistent with the observation that the QCM strongly affects particle transport (figure 1).

4. Comparisons of SOL 'blob' turbulence in L- and H-mode plasmas

We now consider a different aspect of turbulent transport in the edge. This is the intermittent, cross-field transport that is associated with the radial and poloidal propagation of turbulent structures and that has been shown to dominate the total cross-field transport in the SOL [17]. On C-Mod it is studied using probes and GPI. Although the turbulent structures are actually filaments, aligned with the local field, having small $k_{||}$, they have the appearance of 'blobs' when viewed along the field. As an example of the birth and propagation of a blob, we show six consecutive frames from the GPI camera in figure 5. Although the birth *location* of the prominent blob identified in these frames is atypical (and will be discussed in the next section), the blob's size and its outward propagation are typical. The blobs are detected as large amplitude events on the emission signals of the diode array views and as large amplitude ion-saturation-current and floating-potential events by probes. An example of the GPI emission time history from one of the outboard views is shown in figure 6. In the far SOL the 'event' probability distribution function

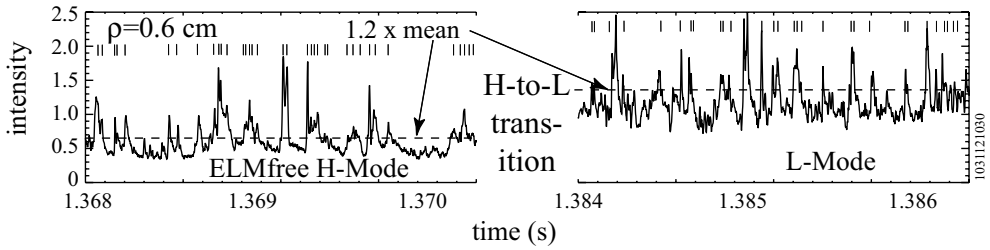

Figure 6. Time history of GPI emission from an outboard view at $\rho = 0.6$ cm (far SOL) during an H-mode period well after the L-to-H transition (left) and during the L-mode period (right) following the H-to-L back transition.

is typically strongly skewed towards larger amplitude events; both skewness and kurtosis are >0. It is important to note that both the GPI diagnostics and the probes show that this turbulence is reduced by a factor of 5 or more on the inboard side compared with the outboard side [18], evidence of its probable ballooning character.

We now turn to a comparison of the SOL blob turbulence in L- and H-modes. Similar studies using probes have been reported in [1, 17, 19]. Figure 6 shows the local emission signal first during an ELMfree period and then during a following L-mode period. The time histories indicate that the nature of the blob turbulence is qualitatively similar in L- and H-modes. Using the outboard GPI diagnostics we will compare quantitatively the spatial size of the blob structures, and the frequency and magnitude of the blob events, as well as discuss observations about their radial propagation velocity. In these comparisons we examine the H-mode after the pedestal has developed and the core density has increased significantly, i.e. not immediately after an L-to-H transition when the GPI diagnostics indicate that the SOL is more quiescent. A measure of the spatial size of the blobs is found from the poloidal correlation lengths of emission in the GPI camera images. Poloidal and radial correlation lengths are similar [7]. The comparison is shown in figure 7(*a*). The shaded areas are the ranges of mean values determined from each sequence of images; approximately 10 sequences, each from a different discharge, were analysed for each confinement mode. Also shown are two characteristic error bars. The larger (dashed) is representative of the standard deviation for a single sequence of images. The smaller error bar (solid) assumes that correlation length at each ρ is the same for the given confinement mode and represents the standard deviation using all of the images analysed for that confinement mode. As shown, correlation lengths of the blobs in the far SOL are somewhat smaller in ELMfree H-mode compared with L-mode. The frequency of the blob events has been determined using the signals from the outboard diode array. In the analysis it is assumed that the blobs sweep past the views and are thus detected as emission spikes above what would be expected from random Gaussian-distributed fluctuations. The frequency of distinguishable events above a threshold is calculated (with the threshold set relative to the mean value of the signal). As illustrated in figure 6 by the tick marks at the top of the figure, this amounts to counting the number of time-series local maxima that are above the threshold. In the case where the threshold is 1.2 times the mean, the frequencies are plotted versus ρ in figure 7(*b*) and are seen to be similar for L-mode and ELMfree H-mode. This result depends somewhat on the

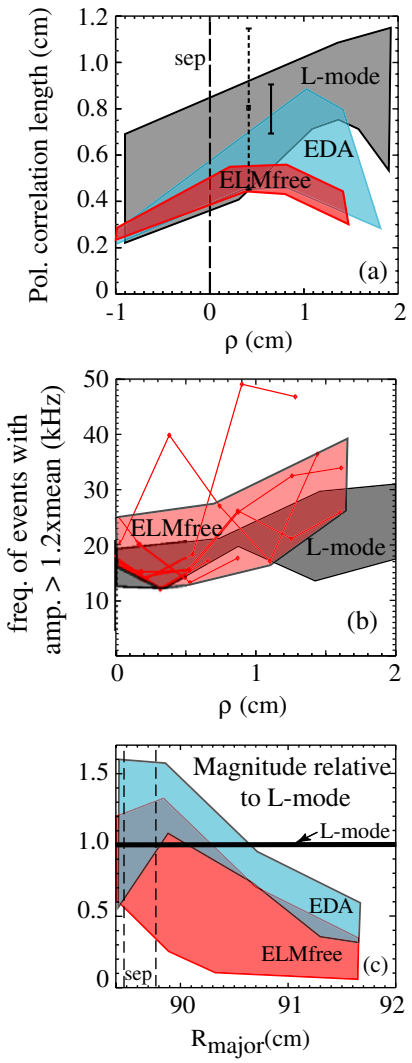

Figure 7. Comparisons of (*a*) blob size (i.e. poloidal correlation length), (*b*) blob frequency and (*c*) blob magnitude versus radius for the different confinement modes. In (*b*) data from single ELMfree H-mode periods are also plotted (as connected line segments). These show some outliers from the range typical for ELMfree H-modes (the light shaded region). In (*c*) abssisa values are the major radii for the views and the dashed lines indicate the range of separatrix locations during the measurement times.

chosen threshold, since the mean value in H-mode is smaller than in L-mode. We conclude, however, that the frequency of blob events with magnitudes greater than this threshold is similar in the two cases. The *magnitudes* of blob events

are compared by examining the integral under those events whose maxima are greater than the threshold, i.e. the integral of the intensity above the threshold. Since in this case we are comparing intensities (and the diode array views are not absolutely calibrated), we compare the magnitudes relative to L-mode for each view separately. This comparison is shown in figure 7(*c*), for which the threshold is also 1.2 times the mean. Here we see a distinct separation between L- and H-mode, with significantly smaller blob magnitudes in the far SOL during ELMfree H-mode as compared with L-mode. The EDA/L-mode comparison shows an intermediate effect. Decreased 'event' magnitudes in H-mode relative to L-mode were also seen in DIII-D [20].

The fluctuation phase velocities can also be compared using a time-delay cross-correlation analysis of the GPI camera images [21]. The velocity fields, which are calculated as time averages over the 1.2 ms of camera data, typically show a mixture of radially outward and poloidal motion outside the separatrix. In the SOL the fluctuations are dominated by blobs, so we assume that the fluctuation phase velocity fields reflect the actual motion of the blobs. In lower single null discharges the dominant poloidal direction in the SOL is downward towards the divertor (ion diamagnetic drift direction). The magnitudes of the radial and poloidal components vary between ~0 and 1000 m s^{-1}. To date we have not found a systematic difference in velocity fields between L- and H-mode. This is primarily because of a wide variation in SOL velocity fields observed for L-mode discharges.

5. 'Blob' turbulence near the density limit

Of particular interest is the generation of the blobs in plasmas near the Greenwald density limit in L-mode discharges. For discharges well below the limit, the typical event distributions around the separatrix and in the near SOL (both from the probe measurements and the optical measurements) are more Gaussian, less skewed towards larger events (i.e. fewer blobs) than is the case in the far SOL [1]. The two-dimensional camera images, which typically show blob generation only outside the separatrix for discharges with $n/n_{GW} < 0.6$, are consistent with this. However, as the density limit is approached, the region of intermittent convective transport expands inwards radially, eventually crossing into the closed flux surfaces. Not coincidently, when that occurs, the levels of cross-field convected *power* are seen to be larger than the power conducted to the divertor, separatrix temperatures and temperature gradients are reduced [1], typically a MARFE appears, the plasma column shrinks and the plasma is abruptly terminated. The observations of blob generation inside the separatrix at densities approaching the limit, as illustrated in figure 5, add further support to this picture. Although it is hard to quantify the spatial distribution of the blob birth locations, we do observe, as is pointed out in [1], the inward expansion of the region of higher fluctuation levels as the limit is approached. Similarly, the region where the skewness values in distributions of emission intensities are large also shifts inwards. The radial profile of normalized GPI emission fluctuations and the associated T_e profiles at two values of normalized density, $n/n_{GW} = 0.33$ and 0.8, are shown in figure 8. For the case near the density limit, fluctuation levels

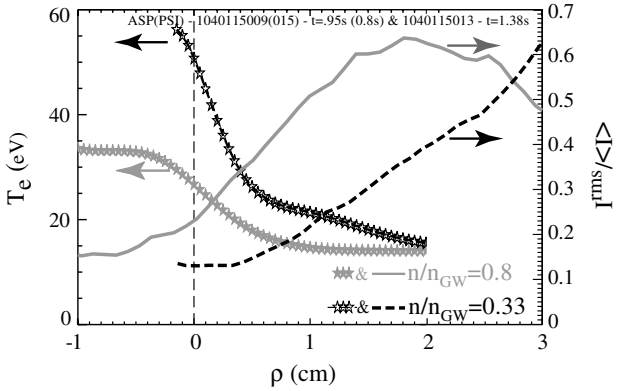

Figure 8. Radial profiles of T_e and normalized emission fluctuations, I^{RMS}/I_{ave}, at two values of n/n_{GW}, 0.33 (black) and 0.8 (grey). The emission fluctuations are in He I. Near the density limit, blobs are seen inside the separatrix (figure 5).

in the $-1 < \rho < 2$ cm region have increased significantly, while T_e and the temperature gradient at the separatrix have decreased. A larger temperature gradient must exist further inside of $\rho = -1$ cm in order to connect to core T_e profiles. Whereas blobs are typically seen only outside the separatrix, *near the density limit, under these conditions, blob generation inside the separatrix is observed* (figure 5). This is indicative that blob generation in C-Mod is associated with gradients rather than with the transition from closed to open field lines.

6. Discussion

A first principles' theoretical description for the QCM does not exist. Experimentally it has been shown to be important in providing the beneficial particle transport that flushes impurities and in providing the opportunity for density control. Since other transport-driving coherent fluctuations that are qualitatively similar to the QCM have been identified on other devices in other transport regimes (e.g. type II ELMy H-mode in Asdex Upgrade [22, 23] and the 'edge harmonic oscillation' in quiescent H-modes [24, 25]), it is important to investigate the common features and the drive for these phenomena. In the QCM case the observed in/out asymmetry in its amplitude provides a clue to its drive. The observation that it extends across the separatrix qualitatively supports its effect on transport. Although the QCM has been shown to exist at the edge of the plasma, there are still differences in what is measured for its typical radial width. The optical diagnostics (GPI and BES) measure a larger width than do the probe and reflectometer, although GPI-probe comparisons made at the same time show good agreement over that part of the profile measured by both. One-dimensional modelling of D_α response to a QCM-like density perturbation yields an amplitude/phase relationship similar to the observation, with the implication that the profile measured by the emission is broadened as a result of ionization 'shadowing' by the perturbation.

Blob generation and transport dynamics [26] are also not fully understood. The in/out asymmetry is indicative of a ballooning-like drive [18]. The comparisons of blob characteristics in L- and H-mode, both here and elsewhere [17, 19], indicate that the blobs are not directly involved with

the physics of the L–H transition, the pedestal formation or its sustainment. While this type of intermittent transport occurs in most tokamaks [27] and stellarators [28], we note differences in some of the details of the blob characteristics. For example, on DIII-D the inferred blob radial velocities are typically in the 1–3 km s^{-1} range [17], not the <1 km s^{-1} range observed on C-Mod. On the other hand the blob generation and transport do appear to play a role in density limit, with blob generation extending into closed flux surfaces as the limit is approached.

Acknowledgments

Work supported at MIT by DoE Coop. Agreement DE-FC02-99ER54512, Contract No DE-AC02-76CHO3073 and Grant DE-FG03-96ER54373.

References

[1] LaBombard B. *et al* 2001 *Phys. Plasmas* **8** 2107
[2] Greenwald M. *et al* 1999 *Phys. Plasmas* **6** 1943
[3] Carreras B. *et al* 2001 *Phys. Plasmas* **8** 3072
[4] Umansky M. *et al* 1998 *Phys. Plasmas* **5** 3373
[5] Terry J.L. *et al* 2001 *J. Nucl. Mater.* **290** 757
[6] Maqueda R.J. *et al* 2001 *Rev. Sci. Instrum.* **72** 931
[7] Zweben S.J. *et al* 2002 *Phys. Plasmas* **9** 1981
[8] Terry J.L. *et al* 2004 *Rev. Sci. Instrum.* **75** 4196
[9] Stotler D. *et al* 2003 *J. Nucl. Mater.* **313–316** 1066
[10] Mazurenko A. *et al* 2002 *Phys. Rev. Lett.* **89** 225004
[11] LaBombard B. *et al* 2000 *Nucl. Fusion* **40** 2041
[12] Hubbard A.E. *et al* 2001 *Phys. Plasmas* **8** 2033
[13] Snipes J.A. *et al* 2001 *Plasma Phys. Control. Fusion* **43** L23
[14] Sampsell M. 2004 *Beam Emission Spectroscopy on the Alcator C-Mod Tokamak PhD Thesis* University of Texas at Austin, submitted
[15] Hughes J.W. *et al* 2002 *Phys. Plasmas* **9** 3019
[16] LaBombard B. 2001 *PSFC Research Report* PSFC/RR-01-3; http://psfcwww2.psfc.mit.edu/library/01rr/01RR003/01RR003_ABS.HTML
[17] Rudakov D.L. *et al* 2002 *Plasma Phys. Control. Fusion* **44** 717
[18] Terry J.L. *et al* 2003 *Phys. Plasmas* **10** 1739
[19] Boedo J.A. *et al* 2001 *Phys. Plasmas* **8** 4826
[20] Boedo J.A. *et al* 2002 *J. Nucl. Mater.* **313–316** 813
[21] Terry J.L. *et al* 2005 *J. Nucl. Mater.* **337–339** 322
[22] Stober J. *et al* 2001 *Plasma Phys. Control. Fusion* **43** A39
[23] Stober J. *et al* 2001 *Nucl. Fusion* **41** 1123
[24] Burrell K.H. *et al* 2002 *Plasma Phys. Control. Fusion* **44** A253
[25] Suttrop W. *et al* 2003 *Plasma Phys. Control. Fusion* **45** 1399
[26] D'Ippolito D.A. and Myra J.R. 2003 *Phys. Plasmas* **10** 4029
[27] Hidalgo C. *et al* 2002 *Plasma Phys. Control. Fusion* **44** 1557
[28] Grulke O. *et al* 2001 *Phys. Plasmas* **8** 5171